Nature, Density, and Catalytic Role of Exposed Species on Dispersed $VO_x/CrO_x/Al_2O_3$ Catalysts

Shuwu Yang, Enrique Iglesia,* and Alexis T. Bell*

Chemical Sciences Division, Lawrence Berkeley National Laboratory, and Department of Chemical Engineering, University of California, Berkeley, California 94720-1462

Received: September 14, 2005

The structure and surface composition of binary oxides consisting of CrO_x and VO_x dispersed on alumina and their effects on the rate and selectivity of oxidative dehydrogenation (ODH) of propane were examined and compared with those for CrO_x and VO_x dispersed on alumina. VO_x deposition on an equivalent CrO_x monolayer on alumina and deposition of CrO_x on an equivalent monolayer of VO_x deposited on alumina led to $CrVO_4$ species during thermal treatment with concomitant reduction of Cr^{6+} to Cr^{3+}. Autoreduction of Cr^{6+} to Cr^{3+} is also detected for CrO_x, even without the presence of VO_x. Infrared spectroscopy of NO adsorbed at 153 K probes the relative abundance of alumina and of V^{5+}, Cr^{3+}, and Cr^{6+} at surfaces. This technique detects differences in the surface composition of $VO_x/CrO_x/Al_2O_3$ and $CrO_x/VO_x/Al_2O_3$. The first of these samples is enriched in VO_x relative to CrO_x compared with the second sample. Consistent with this finding, $VO_x/CrO_x/Al_2O_3$ and $CrO_x/VO_x/Al_2O_3$ are distinguishable in their ODH activities and propene selectivities. The highest ODH activity and propene selectivity is observed for $VO_x/CrO_x/Al_2O_3$, which exhibits a surface enriched in VO_x and having a low surface concentration of Cr^{6+}.

1. Introduction

VO_x/Al_2O_3 is one of the most active and selective catalysts reported for the oxidative dehydrogenation (ODH) of propane to propene,[1−25] but reaction rates and selectivities remain too low for industrial practice. V−O−Al linkages present in VO_x/Al_2O_3 are relatively inactive for ODH reactions but favor secondary combustion of propene to CO and CO_2.[11,26] These undesired V−O−Al linkages can be minimized by placing an intervening layer of another reducible oxide between VO_x and Al_2O_3.[26,27] Specific promotional effects were detected when CrO_x was used as the intervening layer.[27] $VO_x/CrO_x/Al_2O_3$ (VCrAl) gave higher propene rates than VO_x/Al_2O_3; preliminary studies showed that the bilayer structure was disrupted during thermal treatment, leading to partial mixing of VO_x and CrO_x layers, with the resulting formation of V−O−Cr linkages and with significant uncertainty about the extent to which VO_x and CrO_x species were exposed at catalytic surfaces.[27] Both Cr^{3+} and Cr^{6+} were detected in $VO_x/CrO_x/Al_2O_3$, and it seemed that Cr^{6+} favored the primary combustion of propane, which led to low propene selectivity. Thus, there is a need to characterize the surface composition of mixed metal oxide layers in order to establish the effects of surface composition on the activity and selectivity of such catalysts.

Techniques such as Raman spectroscopy, X-ray photoelectron spectroscopy (XPS), X-ray absorption spectroscopy (XAS), and secondary-ion mass spectroscopy (SIMS) cannot give exact information about surface, because these methods probe regions 1−2 nm in depth. In contrast, a suitable probe molecule can adsorb selectively on surfaces and be detected by its characteristic vibration bands. For the $VO_x/CrO_x/Al_2O_3$ system, an appropriate probe should not only distinguish V, Cr, and Al sites but also be sensitive to the vanadium oxidation state (V^{5+}, V^{4+}, V^{3+}) and that of Cr (Cr^{6+}, Cr^{3+}). The previous literature suggests that NO satisfies such requirements and may be useful in the VCrAl system. Therefore, we chose the infrared spectra of adsorbed NO as a probe of surface-exposed V and Cr sites on binary dispersed VCrAl catalysts. NO is able to differentiate the surface V^{5+}, Cr^{6+}, and Cr^{3+} sites. By comparing NO adsorbed on VAl and CrAl with that on an equivalent monolayer of VO_x and CrO_x, the amounts of surface exposed V and Cr sites on VCrAl were measured. These observations are then related to the observed activity and selectivity of VCrAl catalysts for propane ODH.

2. Experimental Section

2.1. Synthesis of Binary Dispersed $VO_x/CrO_x/Al_2O_3$ and $CrO_x/VO_x/Al_2O_3$. CrO_x/Al_2O_3 (CrAl) was prepared by incipient-wetness impregnation of fumed Al_2O_3 (Degussa AG; surface area 125 $m^2\ g^{-1}$) with an aqueous solution of chromium(III) nitrate nonahydrate (Aldrich, 98%). Samples were dried at 383 K in ambient air overnight and then treated in flowing dry air (Airgas, zero grade, 3.33 $cm^3\ s^{-1}$) by raising its temperature from 298 to 773 K at 0.167 K s^{-1} and holding at 773 K for 2 h. VO_x/Al_2O_3 (VAl) samples were prepared by incipient-wetness impregnation of Al_2O_3 with a 2-propanol (Aldrich, 99.99%) solution of vanadyl isopropoxide (Aldrich, 98%). The impregnated alumina was kept in a N_2 flow within a glovebox overnight and then was transferred into a quartz reactor sealed with stopcocks. Samples were treated at 393 K in flowing N_2 (Airgas, 99.999%, 1.67 $cm^3\ s^{-1}$) for 1 h and at 573 K for 1 h; then, air (Airgas, zero grade, 1.67 $cm^3\ s^{-1}$) was introduced, and samples held at 573 K for 1 h and at 773 K for 2 h. Binary dispersed $VO_x/CrO_x/Al_2O_3$ (VCrAl) catalysts were prepared by incipient-wetness impregnation of CrAl with a 2-propanol solution of vanadyl isopropoxide and were subsequently treated in the same manner as VAl. A 12% Cr_2O_3/10% V_2O_5/Al_2O_3 (12Cr10VAl) sample was prepared by incipient-wetness impregnation of 10%

* Corresponding authors. E-mail: bell@cchem.berkeley.edu (A.T.B.); iglesia@cchem.berkeley.edu (E.I.).

10.1021/jp0582538 CCC: $33.50
Published on Web 01/20/2006

TABLE 1: BET Surface Areas and VO_x Surface Densities of 12CrAl, *x*V12CrAl, and *x*VAl Catalysts

catalyst	denotation	wt % V_2O_5	surface area (m^2 g-cat^{-1})	surface area (m^2 g-$Al_2O_3^{-1}$)	VO_x surface density (V nm^{-2})
12% Cr_2O_3/Al_2O_3	12CrAl		120.0	136.4	7.9 (Cr nm^{-2})
3% V_2O_5/12% Cr_2O_3/Al_2O_3	3V12CrAl	3.0[a]	94.8	111.1	2.1
7% V_2O_5/12% Cr_2O_3/Al_2O_3	7V12CrAl	6.4[a]	98.6	119.7	4.3
10% V_2O_5/12% Cr_2O_3/Al_2O_3	10V12CrAl	8.9[a]	93.0	116.0	6.3
3% V_2O_5/Al_2O_3	3VAl	3.1[a]	108.1	111.6	1.9
7% V_2O_5/Al_2O_3	7VAl	7.3[a]	119.3	128.7	4.1
10% V_2O_5/Al_2O_3	10VAl	8.3[a]	103.3	112.6	5.3
12% V_2O_5/Al_2O_3	12VAl	10.5[a]	106.0	118.4	6.5

[a] Obtained by inductively coupled plasma (ICP) analysis.

V_2O_5/Al_2O_3 with an aqueous chromium(III) nitrate solution, followed by drying at 383 K in ambient air and treating in flowing dry air at 773 K for 2 h.

Crystalline bulk $CrVO_4$ was prepared using the method proposed by Touboul and co-workers.[28,29] Nitric acid (3N, EM Science, GR) was added to an aqueous solution of $Cr(NO_3)_3$ and NH_4VO_3 to give a pH of 1 and then was refluxed at 333 K for 6 h. The precipitate was filtered and washed with 300 mL of deionized water**,** dried at 393 K overnight in ambient air, and then treated in flowing dry air (Airgas, zero grade, 1.67 cm^3 s^{-1}) at 1073 K for 6 h. The X-ray diffraction (XRD) pattern of the as-synthesized sample was measured with a Siemens D5000 unit at ambient temperature using CuKα radiation, an X-ray tube operating at 45 kV and 35 mA, and a scan rate of 1.2° min^{-1}. Crystalline $CrVO_4$−I was identified by comparison with literature XRD patterns.[39]

2.2. Catalyst Characterization. BET surface areas were measured by adsorbing N_2 at its normal boiling point using a Quantasorb 6 surface analyzer (Quantachrome Corp.). Samples were treated in a dynamic vacuum (0.1 Pa) at 393 K for more than 3 h before BET measurements. The surface areas for all samples are listed in Table 1.

Raman spectra were measured in a Hololab Series 5000 spectrometer (Kaiser Optical) equipped with a frequency-doubled 75-mW Nd:YAG laser (532 nm). Samples were pressed into self-supported wafers (0.9-cm diameter, ~50 mg cm^{-2}) at 200 MPa and then placed onto a rotating holder held within a quartz cell. Spectra were measured at ambient temperature before and after the treating of the samples in flowing dry air (Airgas, zero grade, 0.83 cm^3 s^{-1}) by heating to 673 K at 0.167 K s^{-1} and holding at 673 K for 1 h.

V and Cr K-edge X-ray absorption spectra (XAS) were recorded in transmission mode using a Si(111) crystal monochromator at the Stanford Synchrotron Radiation Laboratory using beamline 2-3 and an in situ flow cell. All samples were pressed into 10-mm diameter wafers containing ~15 mg cm^{-2} of catalyst. Energy resolutions for the spectra were 5 eV in the preedge region, 0.25 eV in the edge region, and 2.5 eV in the fine structure region. X-ray absorption data were analyzed using IFEFFIT Athena software (version 1.0068). The energy was calibrated using the first inflection point in the spectra for V or Cr foils collected concurrently with each sample spectrum (5465 eV for V and 5989 eV for Cr).

Temperature-programmed reduction (TPR) studies were conducted in a flow QS-10 unit (Quantachrome Corp.). H_2 concentrations were measured using a thermal conductivity detector calibrated by reducing bulk CuO powder (Aldrich, 99.995%). The amount of sample (15−100 mg) was chosen to maintain the same number of oxygen atoms in all experiments. Samples were treated at 1173 K in 20% H_2−Ar (Praxair, 99.999%) at 0.167 K s^{-1} and were held at 1173 K for 1 h. H_2O formed during reduction was removed before thermal conductivity detection using a 13X sieve trap held at ambient temperature.

Oxygen desorption rates during thermal treatment (O_2-TPD) were measured in a flow system using a mass spectrometer (LH INFICON Transpector) to detect O_2. Each sample (100 mg) was placed within a U-shaped quartz cell and treated in flowing 20% O_2−Ar (Praxair, 99.999%, 0.83 cm^3 s^{-1}) at 773 K for 1 h. The samples were then cooled to ambient temperature in this O_2−Ar mixture and flushed with He (Praxair, 99.999%, 0.83 cm^3 s^{-1}) until the 32 amu signal reached constant background levels. Then, the temperature was increased from 298 to 1173 K at 0.167 K s^{-1} and was held at 1173 K for 0.5−1 h.

Infrared spectra were measured in a glass vacuum system using self-supporting wafers (ca. 10 mg cm^{-2}) and a quartz cell. NaCl windows were attached to the cell using silicon glue (Dow Corning 838), which allowed evacuation to $\sim 1 \times 10^{-3}$ Pa. A heater surrounded the stainless steel tube in the central portion of the cell, which allowed the cell to be heated to 873 K or cooled to ~150 K by allowing liquid nitrogen to flow through the stainless steel tube. While heating or cooling the cell, water flowed through a copper tube surrounding the regions near the NaCl windows to minimize thermal shock to the windows and condensation of water vapor. A sample wafer held in a quartz sample holder was placed in the center of the cell. The sample temperature was measured by a K-type thermocouple positioned close to the center of the wafer. Samples were treated in flowing dry air (Praxair, zero grade, 1.67 cm^3 s^{-1}) at 773 K for 1 h, evacuating them at 773 K for 1 h and treating them with pure O_2 (1.3×10^4 Pa) at 773 K for 1 h to remove adsorbed impurities. The samples were cooled to ambient temperature in O_2 and then evacuated. The samples treated in this manner are denoted as *oxidized samples*. After sample pretreatment, the samples were cooled to 153 K in a vacuum before introduction of NO as a probe molecule. NO (Airgas, 99.98%) was purified by vacuum distillation and several freeze−pump−thaw cycles before use. NO was dosed into the quartz cell until its pressure reached 120 Pa. Infrared spectra were recorded at a resolution of 4 cm^{-1} on a Nicolet NEXUS 670 FT-IR spectrometer equipped with an MCT detector with 64 scans in the 4250−400 cm^{-1} region. Difference spectra were obtained by subtracting spectra before NO adsorption at each temperature.

2.3. Catalytic Rates and Selectivity Measurements. Detailed procedures for measurement and analysis of reaction rates and selectivities have been reported previously.[27] Oxidative dehydrogenation rates and selectivities were measured at 583−673 K using a vertical quartz microreactor. Catalyst samples (20−40 mg; 250−500 μm aggregates) were diluted with equal amounts of acid-washed quartz powder (250−500 μm). The reactant mixture consisted of C_3H_8 (13.5 kPa, Airgas, 99.9%) and O_2 (1.7 kPa, Airgas, 99.999%) with He as the balance (Airgas, 99.999%). Reactant and product concentrations were

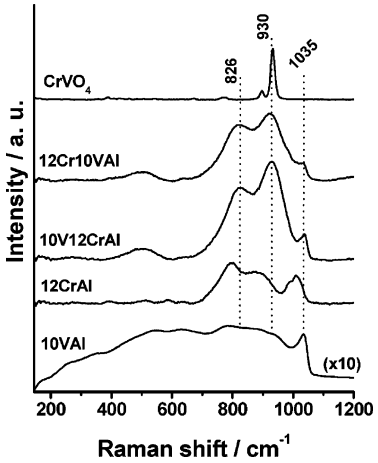

Figure 1. Raman spectra of 10VAl, 12CrAl, 10V12CrAl, and 12Cr10VAl treated in flowing dry air at 673 K for 1 h. The spectrum of $CrVO_4$ is also given as a reference.

measured by gas chromatography (Hewlett-Packard 6890) using a Carboxen 1004 packed column and an HP-PLOT Q capillary column with thermal conductivity and flame ionization detectors, respectively.

3. Results and Discussion

3.1. Structure of VAl, CrAl, VCrAl, and CrVAl. Figure 1 shows Raman spectra for 10VAl, 12CrAl, 10V12CrAl, and 12Cr10VAl and the spectrum for crystalline $CrVO_4$. The spectrum of 10VAl shows bands at 1035, 900, 785, 636, 547, 350, and 266 cm^{-1}, attributed to two types of V-oxo species. The band at 1035 cm^{-1} is assigned to V═O stretches in monovanadates and polyvanadates, while the pairs of broad bands at 900 and 785 cm^{-1}, 636 and 547 cm^{-1}, and 350 and 266 cm^{-1} are attributed to antisymmetric stretches, symmetric stretches, and deformation modes of V−O−V bonds, respectively, in polyvanadate domains of varying size.[27,30] The spectrum of 12CrAl, with an equivalent CrO_x monolayer (7.9 Cr nm^{-2}),[31] shows three intense bands at 1009, 879, and 799 cm^{-1}. The 1009-cm^{-1} band is attributed to Cr═O stretches in isolated monochromates, while the 879 and 799-cm^{-1} bands are assigned to Cr−O−Cr stretches in dichromates and trichromates.[31−34] The weak band at 986 cm^{-1} is assigned to crystalline CrO_3 (bands at 975 and 495 cm^{-1}), but no bands for crystalline Cr_2O_3 (i.e., 550 cm^{-1}) were detected in any of the samples.[30] Upon deposition of VO_x on 12CrAl, the bands at 1009, 986, 879, and 799 cm^{-1} weakened, and when the VO_x deposited reached an equivalent monolayer (10V12CrAl, Figure 1), they were replaced by a band at 1037 cm^{-1}, corresponding to V═O stretches; two broad bands at 930 and 820 cm^{-1} were also observed, and these are assigned below. When an equivalent monolayer of CrO_x was deposited on 10VAl (12Cr10VAl), the spectrum for this sample resembled that for 10V12CrAl.

The band at 930 cm^{-1} resembles that seen in the spectrum of crystalline $CrVO_4$ prepared from $Cr(NO_3)_3$ and NH_4VO_3 (Figure 1), and hence, it is assigned to V−O−Cr stretches.[35,36] In the breadth of this band for 10V12CrAl and 12Cr10VAl and in the absence of $CrVO_4$, diffraction lines for these samples suggest that the $CrVO_4$ domains are disordered and highly dispersed.[27,37−39] The 820 cm^{-1} band may reflect the presence of polychromates, polyvanadates, or mixed V−O−Cr oligomers, but its specific origin remains unclear.

Figure 2 shows X-ray absorption near-edge spectroscopy (XANES) spectra for 10VAl, 12CrAl, 10V12CrAl, and 12Cr10VAl after treatment at 773 K for 2 h in flowing dry air and for three crystalline compounds V_2O_5, CrO_3, Cr_2O_3. The spectrum for V_2O_5 (Figure 2a) has two features (α and β) above the edge, attributable to V_2O_5 crystallites.[40,41] Near-edge spectra for 10VAl, 10V12CrAl, and 12Cr10VAl are similar; they differ clearly from the spectrum of V_2O_5, suggesting the absence of large V_2O_5 crystallites. The preedge feature in 10VAl is slightly more intense than in 10V12CrAl and 12Cr10VAl, indicating that V centers in 10VAl reside in a less centrosymmetric environment than in the other two samples and that the coordination environment of VO_x species in the three samples is influenced by the presence of CrO_x.

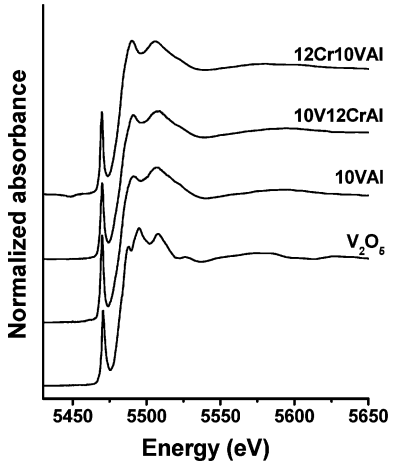

(a) V K-edge

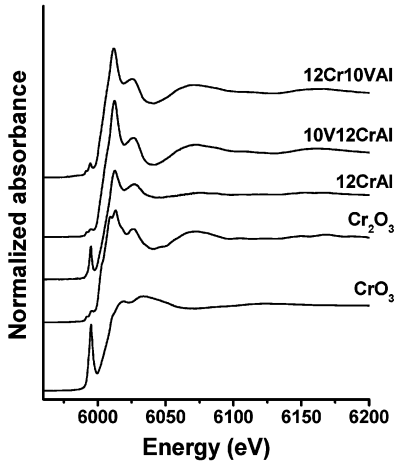

(b) Cr K-edge

Figure 2. Near-edge X-ray absorption spectra of (a) V K-edge of V_2O_5, 10VAl, 10V12CrAl, and 12Cr10VAl; and (b) Cr K-edge of CrO_3, Cr_2O_3, 12CrAl, 10V12CrAl, and 12Cr10VAl.

The Cr near-edge spectrum for CrO_3 shows a sharp preedge feature at ∼5992 eV resulting from dipole-forbidden 1s to 3d transitions that become allowed as a result of orbital hybridization in non-centrosymmetric structures.[42,43] This preedge feature is very weak in the spectrum of Cr_2O_3 (Figure 2b), as it is also for reduced CrO_x.[43] 12CrAl gives a weaker preedge feature than CrO_3, while the preedge and near-edge spectral regions in 10V12CrAl and 12Cr10VAl resemble those in Cr_2O_3, suggesting the predominant presence of Cr^{3+} in these three samples. The amounts of Cr^{3+} in 12CrAl, 10V12CrAl, and 12Cr10VAl were estimated to be ∼50%, >90%, and ∼85%, respectively, using linear superimposition analysis of the preedge region with CrO_3 and Cr_2O_3 as standards; these Cr^{3+} contents are consistent with reduction data presented below.

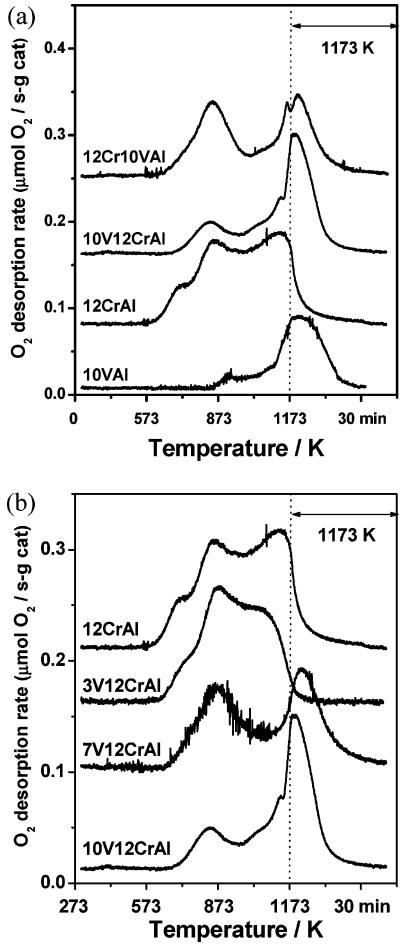

Figure 3. (a) O_2-TPD profiles of 10VAl, 12CrAl, 10V12CrAl, and 12Cr10VAl treated in flowing 20% O_2−Ar at 773 K for 1 h. (b) O_2-TPD profiles of xV12CrAl (x = 3−10) with various VO_x surface densities.

Figure 3 shows the dynamics of O_2 evolution during thermal treatment in He for 10VAl, 12CrAl, 10V12CrAl, and 12Cr10VAl samples pretreated in 20% O_2−Ar at 773 K for 1 h. On 10VAl, O_2 desorbs predominantly above 1173 K, but a small oxygen desorption peak is observed at 923 K. O_2 desorbs from 12CrAl in three peaks at 718, 854, and 1131 K. Raman spectroscopy (Figure 1) suggests that traces of CrO_3 are present in 12CrAl; thus, we suggest that the shoulder at 718 K arises from O_2 desorption from CrO_3 species in 12CrAl, while desorption features at 854 and 1131 K reflect desorption from polychromate domains of varying size.[44]

O_2 desorption peaks for CrO_x (718, 854, and 1131 K) become smaller when an equivalent VO_x monolayer is deposited onto 12CrAl, and a peak appears at >1173 K, as in the case of O_2 desorption from VO_x domains in 10VAl. The low-temperature desorption peaks, characteristic of CrO_x species, were also smaller for 12Cr10VAl than for 12CrAl but larger than for 10V12CrAl samples, again suggesting an effect of deposition sequence on structure and oxygen reactivity. These effects of V on the desorption of O_2 from the CrO_x component reflects the predominant presence of Cr^{3+} in these samples as a result of the formation of $CrVO_4$.

Figure 3b shows the effects of VO_x surface density on the dynamics of O_2 evolution from CrO_x species for 12CrAl and xV12CrAl (x = 3−10) samples with a wide range of VO_x surface densities (1.9−6.5 V nm^{-2}). The intensity of O_2 desorption peaks from CrO_x decreased monotonically with increasing VO_x surface density. These data indicate that the amount of O_2 desorbed from CrO_x (O_2/Cr) also decreased with increasing VO_x surface density (Table 2). Thus, the fraction of the Cr atoms with desorbable oxygens, (e.g., Cr^{6+}) in xV12CrAl decreases with increasing VO_x surface density, because of the concurrent formation of $CrVO_4$.

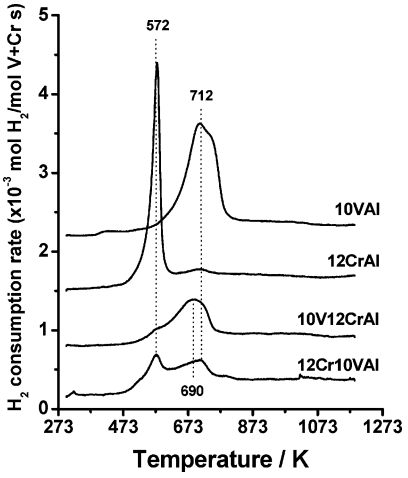

Figure 4. TPR profiles of 10VAl, 12CrAl, 10V12CrAl, and 12Cr10VAl catalysts.

TABLE 2: O_2 Desorbed from CrO_x (mol-O_2 mol-Cr^{-1}) on Each xV12CrAl Sample

sample	O_2/Cr
12CrAl	0.11
3V12CrAl	0.092
7V12CrAl	0.069
10V12CrAl	0.032

Figure 4 shows the dynamics of the reduction in H_2 for 10VAl, 12CrAl, 10V12CrAl, and 12Cr10VAl as a function of temperature. H_2 was consumed in a peak at 712 K with a shoulder at 745 K in 10VAl; these features have been attributed to reduction of V^{5+} to V^{3+} in polyvanadates, based on the measured ratio of H_2 consumed to total amount of VO_x.[16,26,27] The two reduction peaks are consistent with the presence of polyvanadate domains, as also inferred from the Raman spectra (Figure 1). The 12CrAl sample reduces in a peak at 578 K, assigned to Cr^{6+} reduction to Cr^{3+}.[15] Two other H_2 consumption peaks appear at 572 and 690 K for 10V12CrAl and 12Cr10VAl, corresponding to the reduction of Cr^{6+} to Cr^{3+} and V^{5+} to V^{3+}, respectively.[12,26,27] The reduction peak temperature for VO_x species in a binary dispersed sample is lower than that for VAl, indicating that the presence of CrO_x promotes the reduction of VO_x. The reason for this promotional effect of CrO_x is not understood, but it may reflect a change in the electronic properties of VO_x caused by the formation of $CrVO_4$. It should also be noted that the CrO_x reduction peak at 572 K for 10V12CrAl is smaller than that for 12Cr10VAl, indicating that 12Cr10VAl contains a greater concentration of Cr^{6+} than 10V12CrAl.

Figure 5a shows reduction rates (per Cr atom) for 12CrAl and xV12CrAl (x = 3−10). The features for CrO_x reduction become less intense as VO_x surface density increases; in 10V12CrAl, this reduction process appears as a small shoulder next to the VO_x reduction peak, indicating that the fraction of the Cr present as Cr^{6+} in 10V12CrAl is much smaller than in that 12CrAl. All V^{5+} ions in this sample were reduced to V^{3+}.[27] These data confirm that deposition of VO_x on 12CrAl forms dispersed $CrVO_4$ during thermal treatment; all Cr atoms in $CrVO_4$ are trivalent, and V^{5+} ions are more readily reduced than VO_x structures dispersed on Al_2O_3.

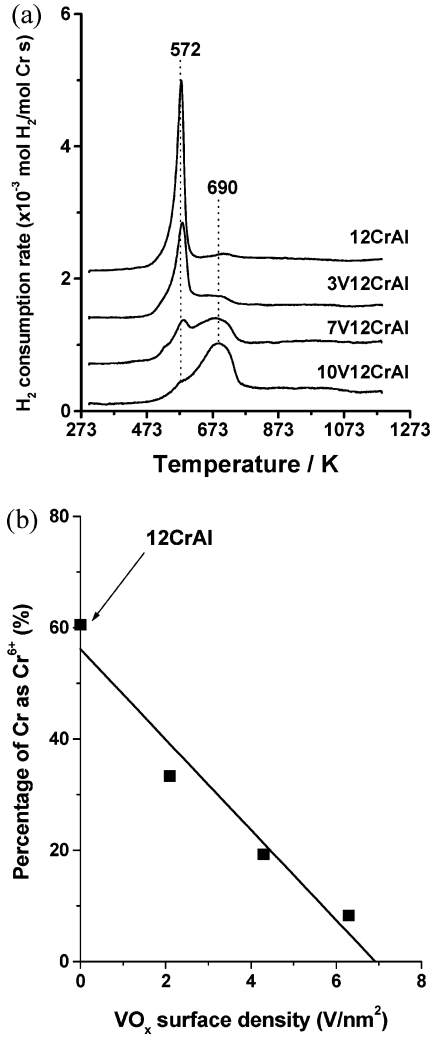

Figure 5. (a) TPR profiles of 12CrAl and *x*V12CrAl ($x = 3-10$) catalysts. (b) Percentage of Cr as Cr^{6+} in 12CrAl, *x*V12CrAl, and 12Cr10VAl catalysts as calculated from TPR data (dividing real value of consumed H_2 by theoretical value). It is assumed that all Cr^{6+} were reduced to Cr^{3+}.

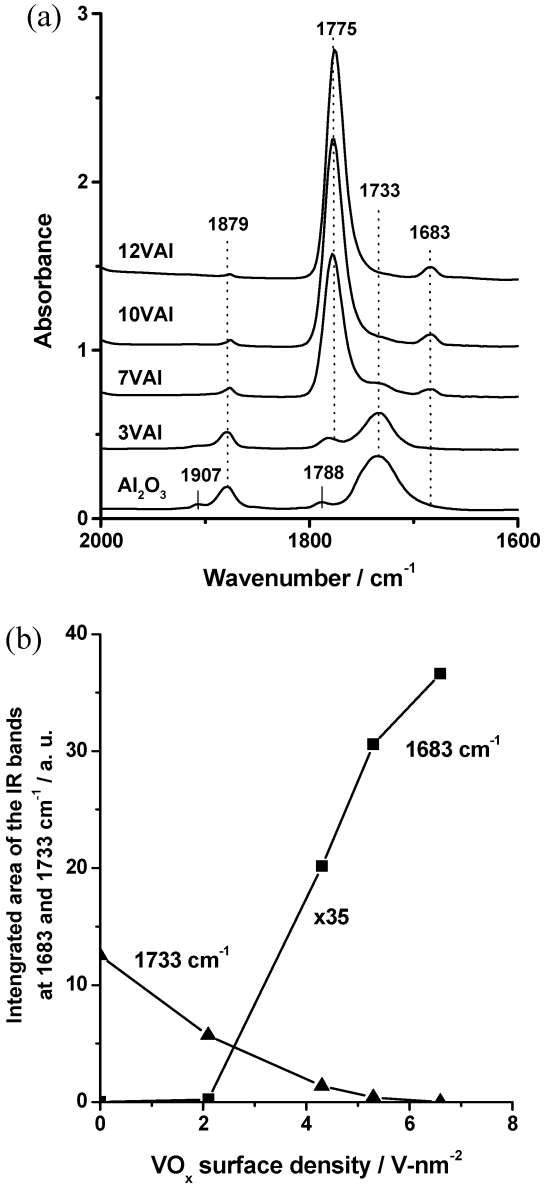

Figure 6. (a) IR spectra of NO adsorbed on oxidized *x*VAl ($x = 3-12$) treated in O_2 (100 Torr) at 773 K for 1 h. (b) Integrated intensities of the IR bands at 1683 and 1733 cm^{-1} in part a as a function of VO_x surface density.

The reduction profiles in Figure 5a were deconvoluted (Gaussian Function and Origin; version 7.0), and individual components were integrated to estimate the amount of H_2 consumed (H_2/Cr) within each reduction peak. These H_2/Cr ratios were divided by the value expected for the reduction of all Cr atoms from Cr^{6+} to Cr^{3+} (Figure 5b), which reflects the fraction of Cr present as Cr^{6+}. Only ~60% of the Cr atoms are present as Cr^{6+} in 12CrAl after thermal treatment in air, suggesting that the autoreduction of CrO_x structures occurred during this treatment. The presence of VO_x favors Cr^{3+} by stabilizing it in $CrVO_4$ structures; only 8% of the Cr atoms are in the Cr^{6+} state in 10V12CrAl, consistent with X-ray absorption and O_2 evolution data.

In summary, Raman and X-ray absorption spectra and O_2 evolution and H_2 consumption dynamics show that Cr^{3+} forms in 12CrAl and VCrAl samples. In the presence of CrO_x, VO_x species are more readily reduced than in VO_x-only structures dispersed on Al_2O_3. The deposition sequence of VO_x and CrO_x influenced the structure and oxygen reactivity of binary VCr oxides dispersed on Al_2O_3.

3.2. Surface Composition of VCrAl and CrVAl and Relationship to Catalyst Activity and Selectivity. NO was used to prove the nature and number of V and Cr species exposed at surfaces. NO adsorbs strongly on V^{3+} or V^{4+} or both but adsorbs much more weakly on V^{5+} at ambient temperature.[45-48] Since only V^{5+} is present in the materials of interest for this study, NO was adsorbed at 153 K. Figure 6a shows infrared spectra for NO adsorbed at 153 K on Al_2O_3 and *x*VAl ($x = 3-12$, 1.9−6.5 V nm^{-2}). Four bands are observed at 1907, 1879, 1788, and 1733 cm^{-1} that can be assigned to *cis*-ONNO dimers (O═N−N═O) based their positions.[49,50] The infrared bands for NO dimers on Al_2O_3 are observed on 3VAl (1.9 V nm^{-2}), but their intensities are slightly lower than those on pure Al_2O_3. Infrared bands for NO adsorbed on V^{5+} appear at 1683 and 1775 cm^{-1}. The bands for NO dimers on Al_2O_3 become weaker as the VO_x surface density increases and cannot be detected above 6.5 V nm^{-2}; the two bands at 1775 and 1683 cm^{-1} become stronger as the VO_x surface density increases. The concurrent increase in the intensity of these two bands lead us to assign them to the same structure, specifically to the formation of antisymmetric NONO dimers (N═O···N═O) adsorbed on VO_x.[50]

The integrated area of the band at 1683 cm^{-1} is shown as a function of the VO_x surface density in Figure 6b. The intensity

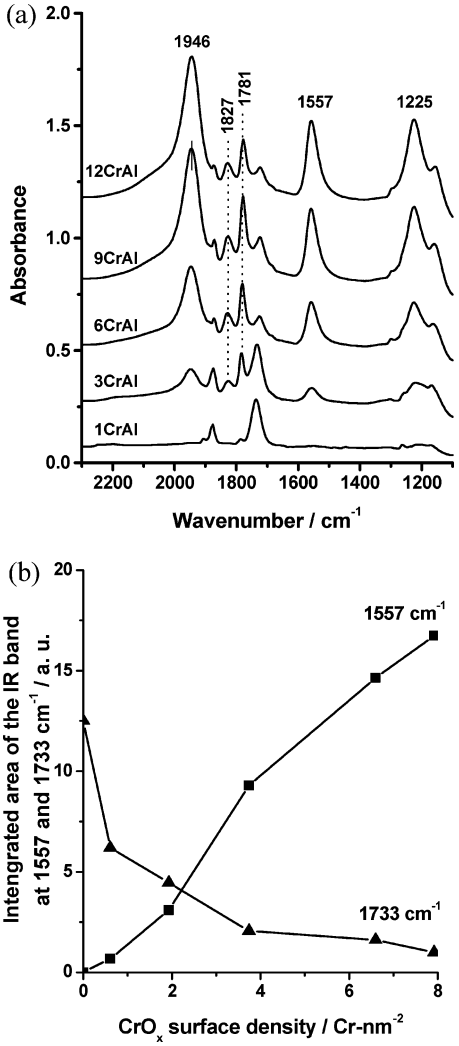

Figure 7. (a) IR spectra of NO adsorbed on oxidized *x*CrAl ($x = 1-12$) treated in O_2 (100 Torr) at 773 K for 1 h. (b) Integrated intensities of the IR bands at 1557 and 1733 cm^{-1} in part a as a function of CrO_x surface density.

of this feature is nearly zero for VO_x surface densities below 3 V nm^{-2} but then increased linearly with increasing VO_x surface density in the range of 3−7 V nm^{-2}. Raman spectra showed that monovanadates predominate for VAl samples with < 3 V nm^{-2}, while polyvanadates increased in concentration as surface densities increased above 3 V nm^{-2}. Thus, ONON dimers appear to form only on polyvanadate species. The integrated intensities for the band at 1733 cm^{-1} are also shown in Figure 6b. The intensity of this band decreased monotonically with increasing VO_x surface density, as expected from the gradual coverage of Al_2O_3 surfaces and the concomitant reactions of OH groups with V-oxyhydroxide species during deposition and thermal treatment.

Infrared spectra for NO adsorbed on CrO_x/Al_2O_3 differed from those on VO_x/Al_2O_3. The 1CrAl (0.6 Cr nm^{-2}) sample shows four bands at 1907, 1879, 1788, and 1733 cm^{-1} due to NO adsorption on Al_2O_3 (Figure 7a). Three weak bands at 1946, 1557, and 1225 cm^{-1} were also detected in this sample. The bands for NO adsorbed on Al_2O_3 became weaker and the bands at 1946, 1557, and 1225 cm^{-1} strengthened with increasing CrO_x surface density. Concurrently, complex spectral features became evident in the region of 1900−1700 cm^{-1}. The bands at 1557 and 1225 cm^{-1} have been attributed to the formation of nitrate species by the reaction of Cr^{6+} with NO,[51,52] via the reaction $Cr^{6+} + NO + 2O^{2-} \rightarrow Cr^{3+} + NO_3^-$, which reduces Cr^{6+} to Cr^{3+} while oxidizing N^{2+} to N^{5+}. The positions of these bands lead to their assignment to bidentate nitrates. The band at 1950−1930 cm^{-1} is attributed to NO^+ species.[51] The bands at 1870 and 1750 cm^{-1} are assigned to $Cr^{3+}(NO)_2$ species, as in the case of NO adsorbed on CrO_x/Al_2O_3 treated with H_2 at 673 K (not shown here). The band at 1781 cm^{-1} arises from Cr^{3+}-(NO),[53] and that at 1827 cm^{-1} arises from mononitrosyl species on Cr^{3+} or Cr^{2+}.[53,54] The integrated areas of the bands at 1557 and 1733 cm^{-1} are shown in Figure 7b as a function of CrO_x surface density. The intensity of the band at 1733 cm^{-1} decreases with increasing CrO_x surface density, and the intensity of the band at 1557 cm^{-1} band increases concurrently.

Infrared spectra for NO adsorbed on 12VAl (6.5 V nm^{-2}), 12CrAl, 10V12CrAl (6.3 V nm^{-2}), and 12Cr10VAl samples treated in dry air at 773 K for 1 h are shown in Figure 8a. The infrared bands for NO dimers on V^{5+} and for NO_3^- species on Cr^{6+} are well-resolved on 10V12CrAl and 12Cr10VAl. Clearly, the bands at 1775 and 1683 cm^{-1} were stronger in the spectrum for 10V12CrAl than in that for 12Cr10VAl, but those at 1950, 1555, and 1225 cm^{-1} were more intense for 12Cr10VAl than for 10V12CrAl. The ratio of integrated intensities for the infrared bands at 1775 and 1555 cm^{-1}, I_{1775}/I_{1555}, is 12.8 for 10V12CrAl but only 2.3 for 12Cr10VAl, suggesting that more V^{5+} sites are exposed when VO_x is deposited on $CrO_x-Al_2O_3$ than when the deposition sequence is reversed. The deposition of CrO_x onto $VO_x-Al_2O_3$ leads, in turn, to the preferential exposure of Cr species at surfaces. Thus, samples retain some surface preference for the species deposited last, even if thermal treatment causes some partial mixing within bilayers.

Figure 8b shows infrared spectra for NO adsorbed on *x*V12CrAl ($x = 3-10$, 2.1−6.3 V nm^{-2}) treated in flowing dry air at 773 K for 1 h. The bands at 1775 and 1683 cm^{-1} for NO dimers on V^{5+} increased with increasing VO_x surface density, while the nitrate bands at 1557 and 1225 cm^{-1} concurrently decreased, even though all samples contain similar amounts of Cr. The intensities of the bands at 1683 cm^{-1} (NO dimers on V^{5+}) and 1557 cm^{-1} (nitrates on Cr^{6+}) are shown in Figure 8c as a function of the VO_x surface density. The band at 1557 cm^{-1} for nitrate species on Cr^{6+} decreased linearly, consistent with the decreasing fraction of Cr^{6+} inferred from spectroscopic and chemical analyses (e.g., Figure 5b). In contrast, the band at 1683 cm^{-1} for NO dimers on V^{5+} sites increased monotonically with increasing VO_x surface density.

The assumption that the surface of Al_2O_3 is entirely covered by VO_x species for 12VAl, which contains a theoretical monolayer of polyvanadate species, and by CrO_x in 12CrAl, which contains a theoretical monolayer of polychromate species, allows estimates of the percentage of the alumina surface covered by V^{5+} and Cr^{6+} in other samples. These estimates are obtained by comparing the integrated areas for the 1683 and 1557 cm^{-1} bands in each *x*V12CrAl sample with those for 12VAl and 12CrAl (Figure 8c) and are reported in Table 3. Clearly, CrO_x species predominate on the surface of samples with a low VO_x surface density, while VO_x species become more abundant as the VO_x surface density increases.

V−O−Cr bands in the Raman spectra (Figure 1) indicate that VO_x and CrO_x mix in VCrAl. For 10V12CrAl, containing equivalent monolayers of both CrO_x and VO_x, perfect mixing would lead to ∼50% VO_x coverage on the alumina surface. Instead, we detect enrichment by VO_x (68% VO_x, Table 3), suggesting that mixing is incomplete and that the oxide deposited last remains preferentially exposed. On the basis of the NO adsorption data listed in Table 3 and the VO_x surface

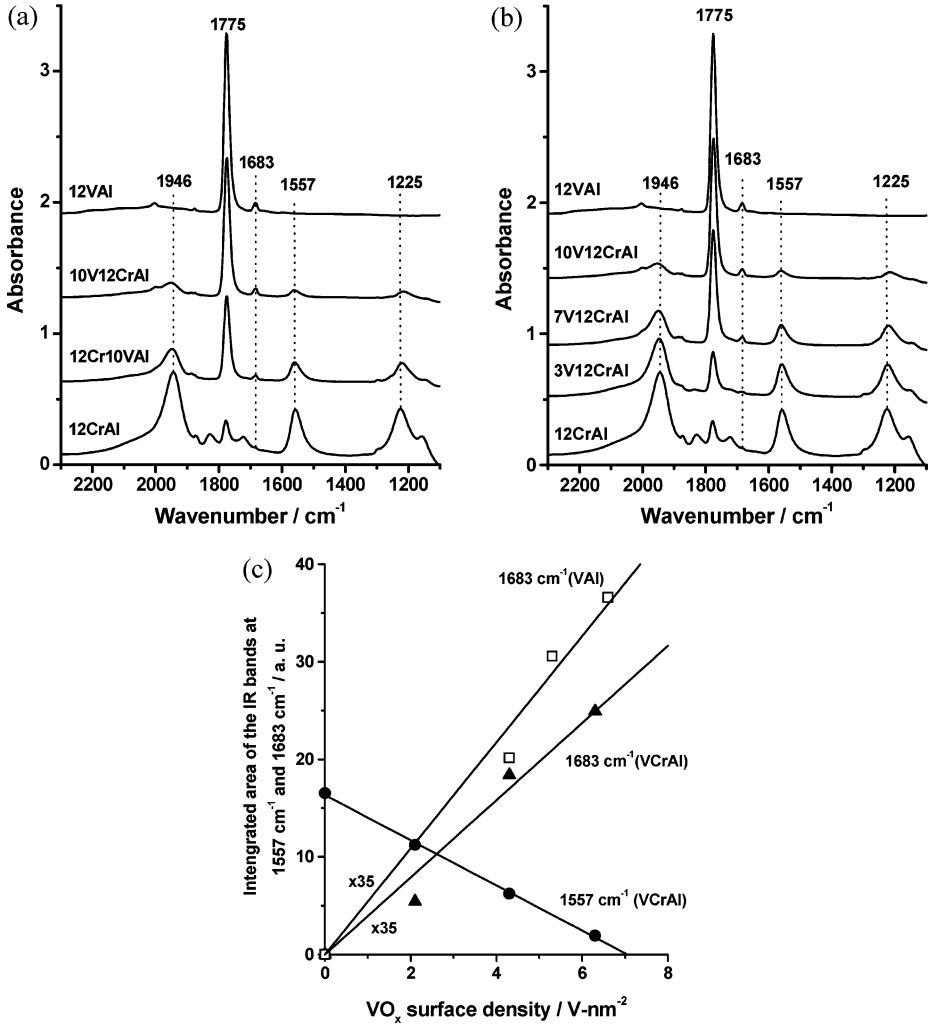

Figure 8. (a) IR spectra of NO adsorbed on oxidized 12VAl, 12CrAl, 10V12CrAl, and 12Cr10VAl treated in O_2 (100 Torr) at 773 K for 1 h. (b) IR spectra of NO adsorbed on oxidized *x*V12CrAl ($x = 3-10$) treated in O_2 (100 Torr) at 773 K for 1 h. (b) Integrated intensities of the IR bands at 1683 cm^{-1} (NO dimer on V site) and 1557 cm^{-1} (nitrate on Cr site) in part b as a function of VO_x surface density. For comparison, the integrated intensities of the IR bands at 1683 cm^{-1} for 10VAl and 12VAl samples are also shown.

TABLE 3: Percentage of Surface Exposed VO_x, Cr^{6+}, and Cr^{3+} on Different Catalysts Determined from IR and NO Adsorption Results

sample	surf covered by VO_x	surf covered by Cr^{6+}	surf covered by Cr^{3+}	VO_x/CrO_x mixing
12CrAl		60%	40%	
3V12CrAl	15%	41%	44%	~35%
7V12CrAl	50%	23%	27%	~33%
10V12CrAl	68%	7%	25%	~64%
12VAl	100%			

densities given in Table 1 and assuming that only 50% VO_x will be accessed by NO if VO_x mixes with CrO_x to form a mixed compound like $CrVO_4$, the extents of VO_x/CrO_x mixing for 3V12CrAl, 7V12CrAl, and 10V12CrAl are estimated to be ~35%, ~33%, and ~64%, respectively.

The rates and primary selectivities for oxidative dehydrogenation of propane on 12CrAl, 12VAl, 10V12CrAl, and 12Cr10VAl are compared in Table 4, which also shows the percentages of the surface covered by V^{5+} and Cr^{6+}/Cr^{3+}. The last two catalysts, similar in composition and in Raman and X-ray absorption spectra, give very different ODH rates and selectivities. ODH rates on 10V12CrAl are ~50% higher than on 12Cr10VAl, and 10V12CrAl also gives higher primary ODH selectivities. These observations reflect a higher accessibility of VO_x, which has a higher primary selectivity, at the surface of 10V12CrAl. Reactions of VO_x with CrO_x to form a mixed oxide, such as $CrVO_4$, lead to higher ODH rates and to lower propane combustion selectvities. Indeed, 12CrAl, which contains the highest fraction of Cr^{6+}, also gives the lowest primary ODH selectivity.

4. Conclusions

Samples of CrAl undergo autoreduction of CrO_x species during calcination, resulting in the appearance of Cr^{3+} cations.

TABLE 4: Percentage of Surface Exposed VO_x, Cr^{6+}, and Cr^{3+} on Different Catalysts Determined from IR and NO Adsorption Results and Their Propane ODH Rates and Selectivity at 583 K

sample	surf covered by VO_x	surf covered by Cr^{6+}	surf covered by Cr^{3+}	primary formation rate of C_3H_6 at 583 K (μmol g^{-1} s^{-1})	primary C_3H_6 selectivity at 583 K
12CrAl		60%	40%	0.68	34%
12VAl	100%			0.89	93%
10V12CrAl	68%	7%	25%	1.13	87%
12Cr10VAl	37%	23%	40%	0.76	39%

In the case of VCrAl, VO_x reacts with CrO_x to form $CrVO_4$, thereby facilitating the reduction of Cr^{6+} to Cr^{3+}. With increasing VO_x surface density, the amount of Cr^{6+} in VCrAl decreases monotonically. NO is a good probe for distinguishing between V and Cr sites at the surface of the binary oxide. Antisymmetric ONON dimers are formed on V^{5+}, and nitrate species are formed on Cr^{6+}, while dinitrosyls are formed on Cr^{3+}. These species have bands at different frequencies, and as a result, surface exposed V and Cr sites could be identified. Partial mixing of VO_x with CrO_x was demonstrated by NO adsorption. Examination of NO adsorption on VCrAl samples by altering the sequence of VO_x and CrO_x deposition suggests that binary dispersed VCr catalysts have a memory of the last deposited species. Thus, $VO_x/CrO_x/Al_2O_3$ exhibits an enhancement in the VO_x present at the surface of the binary oxide relative to $CrO_x/VO_x/Al_2O_3$, and the latter sample exhibits an enhancement in CrO_x relative to the former sample. The catalytic activity and selectivity of VCr binary oxide catalysts is also dependent on the order in which the oxides are deposited. The ODH activity and propene selectivity of $VO_x/CrO_x/Al_2O_3$ are noticeably higher than those of $CrO_x/VO_x/Al_2O_3$, reflecting the differences in the surface composition of the two types of catalysts. The formation of $CrVO_4$ appears to enhance catalyst activity relative to VO_x alone, and the minimization of Cr^{6+} at the catalyst contributes to the attainment of a high primary selectivity to propene.

Acknowledgment. This work was supported by the Director, Office of Basic Energy Sciences, Chemical Sciences Division of the US Department of Energy under Contract DE-AC03-76SF00098. X-ray absorption data were collected at the Stanford Synchrotron Radiation Laboratory, which is operated by the Department of Energy, Office of Basic Energy Sciences, under Contract DE-AC02-05CH11231. We thank Prof. Kazunari Domen and Dr. Junko N. Kondo of the Tokyo Institute of Technology for providing us with the low-temperature infrared cell used for this study.

References and Notes

(1) Kung, H. H. *Adv. Catal.* **1994**, *40*, 1.
(2) Albonetti, S.; Cavani, F.; Trifiro, F. *Catal. Rev.−Sci. Eng.* **1996**, *38*, 413.
(3) Cavani, F.; Koutyrev, M.; Trifiro, F.; Bartolini, A.; Ghisletti, D.; Iezzi, R.; Santucci, A.; Del Piero, G. *J. Catal.* **1996**, *158*, 236.
(4) Blasko, T.; López Nieto, J. M. *Appl. Catal., A* **1997**, *157*, 117.
(5) Khodakov, A.; Yang, J.; Su, S.; Iglesia, E.; Bell, A. T. *J. Catal.* **1998**, *177*, 343.
(6) Khodakov, A.; Olthof, B.; Bell, A. T.; Iglesia, E. *J. Catal.* **1999**, *181*, 205.
(7) Chen, K.; Khodakov, A.; Yang, J.; Bell, A. T.; Iglesia, E. *J. Catal.* **1999**, *186*, 325.
(8) Chen, K.; Bell, A. T.; Iglesia, E. *J. Phys. Chem. B* **2000**, *104*, 1292.
(9) Olthof, B.; Khodakov, A.; Bell, A. T.; Iglesia, E. *J. Phys. Chem. B* **2000**, *104*, 1516.
(10) Chen, K.; Iglesia, E.; Bell, A. T. *J. Catal.* **2000**, *192*, 197.
(11) Argyle, M. D.; Chen, K.; Bell, A. T.; Iglesia, E. *J. Catal.* **2002**, *208*, 139.
(12) Chen, K.; Bell, A. T.; Iglesia, E. *J. Catal.* **2002**, *209*, 35.
(13) Garcia Cortez, G.; Fierro, J. L. G.; Banares, M. A. *Catal. Today* **2003**, *78*, 219.
(14) Grabowski, R.; Sloczynski, J.; Grzesik, N. M. *Appl. Catal., A* **2003**, *242*, 297.
(15) Cherian, M.; Gupta, R.; Rao, M. S.; Deo, G. *Catal. Lett.* **2003**, *86*, 179.
(16) Cherian, M.; Rao, M. S.; Deo, G. *Catal. Today* **2003**, *78*, 397.
(17) Jibril, B. Y.; Al-Zahrani, S. M.; Abasaeed, A. E.; Hughes, R. *Catal. Commun.* **2003**, *4*, 579.
(18) Jibril, B. Y.; Al-Zahrani, S. M.; Abasaeed, A. E.; Hughes, R. *Catal. Lett.* **2003**, *3−4*, 121.
(19) Al-Zahrani, S. M.; Jibril, B. Y.; Abasaeed, A. E. *Catal. Lett.* **2003**, *85*, 57.
(20) Jibril, B. Y. *Appl. Catal. A* **2004**, *264*, 193.
(21) Routray, K.; Reddy, K. R. S. K.; Deo, G. *Appl. Catal., A* **2004**, *265*, 103.
(22) Ballarini, N.; Cavani, F.; Cericola, A.; Cortelli, C.; Ferrari, M.; Trifiro, F.; Capannelli, G.; Comite, A.; Catani, R.; Cornaro, U. *Catal. Today* **2004**, *91−92*, 99.
(23) Grabowski, R. *Appl. Catal., A* **2004**, *270*, 37.
(24) De, M.; Kunzru, D. *Catal. Lett.* **2004**, *96*, 33.
(25) Pieck, C. L.; Banares, M. A.; Fierro, J. L. G. *J. Catal.* **2004**, *224*, 1.
(26) Dai, H.; Bell, A. T.; Iglesia, E. *J. Catal.* **2004**, *221*, 491.
(27) Yang, S.; Bell, A. T.; Iglesia, E. *J. Phys. Chem. B* **2005**, *109*, 8987.
(28) Touboul, M.; Melghit, K. *J. Mater. Chem.* **1995**, *5*, 147.
(29) Baudrin, E.; Denis, S.; Orsini, F.; Seguin, L.; Touboul, M.; Tarascon, J.-M. *J. Mater. Chem.* **1999**, *9*, 101.
(30) Vuurman, M. A.; Wachs, I. E. *J. Phys. Chem.* **1992**, *96*, 5008.
(31) Yang, G.; Haibo, Z.; Biying, Z. *J. Mater. Sci.* **2000**, *35*, 917.
(32) Weckhuysen, B. W.; Wachs, I. E.; Schoonheydt, R. A. *Chem. Rev.* **1996**, *96*, 3327.
(33) Deo, G.; Wachs, I. E. *J. Phys. Chem.* **1991**, *95*, 5889.
(34) Vuurman, M. A.; Stufkens, D. J.; Oskam, A.; Moulijn, J. A.; Kapteijn, F. *J. Mol. Catal.* **1990**, *60*, 83.
(35) Owen, O. S.; Kung, H. H. *J. Mol. Catal.* **1993**, *79*, 265.
(36) Briand, L. E.; Jehng, J.-M.; Cornaglia, L.; Hirt, A. M.; Wachs, I. E. *Catal. Today* **2003**, *78*, 257.
(37) Baran, E. J. *J. Mater. Sci.* **1998**, *33*, 2479.
(38) Baudrin, E.; Denis, S.; Orsini, F.; Seguin, L.; Touboul, M.; Tarascon, J.-M. *J. Mater. Chem.* **1999**, *9*, 101.
(39) Song, Z.; Matsushita, T.; Shishido, T.; Takehira, K. *J. Catal.* **2003**, *218*, 32.
(40) Zhang, S. G.; Higashimoto, S.; Yamashita, H.; Anpo, M. *J. Phys. Chem. B* **1998**, *102*, 5590.
(41) Anpo, M.; Zhang, S. G.; Higashimoto, S.; Matsuoka, M.; Yamashita, H. *J. Phys. Chem. B* **1999**, *103*, 9295.
(42) Bordiga, S.; Bosherini, F.; Coluccia, S.; Genoni, F.; Lamberti, C.; Leofanti, G.; Marcheses, L.; Petrini, G.; Vlaic, G.; Zecchina, A. *Catal. Lett.* **1994**, *26*, 195.
(43) Weckhuysen, B. M.; Schoonheydt, R. A.; Jehng, J.-M.; Wachs, I. E.; Cho, S. J.; Ryoo, R.; Kijlstra, S.; Poels, E. *J. Chem. Soc., Faraday Trans.* **1995**, *91*, 3245.
(44) Grzybowska, B.; Sloczynski, J.; Grabowski, R.; Wcislo, K.; Kozlowska, A.; Stoch, J.; Zielinski, J. *J. Catal.* **1998**, *178*, 687.
(45) Davydov, A. In *IR Spectroscopy of Adsorbed Species on the Surface of Transition Metal Oxides*; Rochester, C. H., Ed.; Wiley: Chichester, **1990**.
(46) Davydov, A. *Kinet. Catal.* **1993**, *34*, 1056.
(47) Dines, T. J.; Rochester, C. H.; Ward, A. M. *J. Chem. Soc., Faraday Trans.* **1991**, *87*, 1617.
(48) Davydov, A. *Russ. Chem. Bull.* **1994**, *43*, 214.
(49) Laane, J.; Ohlsen, J. R. *Prog. Inorg. Chem.* **1986**, *28*, 465.
(50) Hadjiivanov, K.; Concepción, P.; Knözinger, H. *Top. Catal.* **2000**, *11−12*, 123.
(51) Mihaylov, M.; Penkova, A.; Hadjiivanov, K.; Knözinger, H. *J. Phys. Chem. B* **2004**, *108*, 679.
(52) Schraml-Marth, M.; Wokaun, A.; Baiker, A. *J. Catal.* **1992**, *138*, 306.
(53) Ghiotti, G.; Chiorino, A. *Spectrochim. Acta* **1993**, *49A*, 1345.
(54) Ghiotti, G.; Garrone, E,; Gatta G. D.; Fubini, B.; Giamello, E. *J. Catal.* **1983**, *80*, 249.